PRAMANA — journal of physics

Vol. 80, No. 3
March 2013
pp. 487–505

Analysis of thermal distribution in two end pumping Nd:YAG laser rod using bacterial foraging optimization algorithm

MOHAMMED A MINSHED
Laser and Optoelectronics Engineering Department, University of Technology, Baghdad, Iraq
E-mail: dr.mohhamedwhab@gmail.com

MS received 19 March 2012; revised 16 August 2012; accepted 18 September 2012

Abstract. There is a strong need for the optimized management of the thermal problem in Nd:YAG laser rod and for a powerful, fast, and accurate modelling tool capable of treating the heat source distribution very close to what it actually is. In this paper, a new optimization algorithm called bacterial foraging optimization algorithm (BFOA) is proposed for simulation of the radial heat distribution. A BFOA discloses a simulation method which delivers the exact temperature distribution in a circularly cylindrical structure with a circularly symmetrical, longitudinally, and transversally non-uniform heat source distribution and circularly symmetrical cooling means. The output power is obtained and compared with previously published experimental measurements for different pump power and a good agreement has been found.

Keywords. Solid-state lasers; thermal distribution; bacterial foraging; optimization algorithm.

PACS Nos 44.05.e; 42.55.xi; 02.70.−c

1. Introduction

Some new approaches and technical implementations have been proposed for diode pumped solid-state lasers (DPSSLs). However, basically, physics of the problem has remained the same. Typical routes of the control of thermal effects in DPSSLs can be divided into three groups:

(1) Improvement in gain media technology.
(2) New designs of pumping schemes and resonators.
(3) Improvement in cooling techniques [1].

The analytical expressions obtained for the temperature distribution open the way to a better physical understanding of thermal phenomena and represent a fast tool for solid-state laser design and optimization [2]. Optimization is associated with almost every problem of engineering. The underlying principle in optimization is to enforce constraints that

DOI: 10.1007/s12043-012-0496-x; ***e*Publication: 22 February 2013**

must be satisfied while exploring as many options as possible within the trade-off space. There exist numerous optimization techniques. Bio-inspired or nature-inspired optimization techniques are a class of random search techniques suitable for linear and nonlinear processes. Hence, nature-based computing or nature computing is an attractive area of research. Like nature-inspired computing, their application areas are also numerous. To list a few, the nature computing applications include optimization, data analysis, data mining, computer graphics and vision, prediction and diagnosis, design, intelligent control, and traffic and transportation systems. Most of the real life problems occurring in the field of science and engineering may be modelled as nonlinear optimization problems, which may be unimodal or multimodal. Multimodal problems are generally considered more difficult to solve because of the presence of several local and global optima. Bacterial foraging optimization proposed in 2002 by Passino is based on the foraging behaviour of *Escherichia Coli* (*E. coli*) bacteria present in the human intestine [3]. There are many species of bacteria that evidently perform some type of optimization during their motile behaviour. Some optimize their position based on other chemicals, and others based on non-chemical stimuli (e.g. light, magnetism, or heat). Each of these holds the potential for creating a bio-inspired optimization method [4]. In this paper a rate modelling tool capable of treating realistic heat source distribution is presented. The objective and motivation of this paper are to study thermal distribution in laser rod in a more efficient and matching way between BFOA and thermal distribution problem in laser rod.

2. Temperature distribution

The achievement of high power laser systems with high beam quality is largely compromised by thermal effects in the gain medium, which are responsible for thermal lensing, depolarization losses, and ultimately fracture [5]. The equations governing the temperature distribution are given by:

(1) The heat diffusion equations in cylindrical coordinates

(i) *Originating from the pump beam*

$$\frac{\partial^2 T_{\mathrm{p}}(r,t)}{\partial r^2} + \frac{1}{r}\frac{T_{\mathrm{p}}(r,t)}{\partial r} + \frac{1}{k}Q_{\mathrm{p}}(r,t) = \frac{1}{\alpha}\frac{\partial T_{\mathrm{p}}(r,t)}{\partial t}. \tag{1}$$

(ii) *Originating from the laser radiation*

$$\frac{\partial^2 T_{\mathrm{L}}(r,z,t)}{\partial r^2} + \frac{1}{r}\frac{T_{\mathrm{L}}(r,z,t)}{\partial r} + \frac{\partial^2 T_{\mathrm{L}}(r,z,t)}{\partial z^2} + \frac{1}{k}Q_{\mathrm{L}}(r,z,t) = \frac{1}{\alpha}\frac{\partial T_{\mathrm{L}}(r,z,t)}{\partial t}. \tag{2}$$

(2) The boundary condition describing the cooling at the outer radius of the rod

$$-k\frac{\partial T_t(r,z,t)}{\partial r}\bigg|_{r=R} = hT_t(r,z,t)\bigg|_{r=R}, \tag{3}$$

with

$$T_t(r, z, t) = T_{\mathrm{L}}(r, z, t) + T_{\mathrm{p}}(r, t)\,,$$

where $Q_{\mathrm{p}}(r, t)$ is the rate of energy generated from the absorbed part of the pump beam per unit volume, $Q_{\mathrm{L}}(r, z, t)$ is the rate of energy generated from the absorbed part of the amplified laser radiation per unit volume, k is the thermal conductivity of the material, $T_{\mathrm{L}}(r, z, t)$ is the temperature distribution generated from the absorbed part of the amplified laser beam, $T_{\mathrm{p}}(r, t)$ is the temperature distribution generated from the absorbed pump radiation, $\alpha = k/(\rho C_{\mathrm{p}})$ is the thermal diffusivity of the material, ρ is the mass density of the material, C_{p} is the specific heat of the material at constant pressure and h is the heat transfer coefficient [6]. It is often useful to know how the optical absorption depth compares with the thermal diffusion distance during a laser irradiation. To see the meaning of the thermal diffusion depth more clearly, consider the following particular solutions of eq. (2):

$$T(z, t) = \frac{I T_{\mathrm{p}} \alpha}{2\rho C(\pi)^{1/2}} \frac{\mathrm{e}^{-z^2/4\alpha t}}{(4\alpha t)^{1/2}}, \qquad \text{for } t > 0. \tag{4}$$

The important role of the quantity z_{D} which is equal to $(4\alpha t)^{1/2}$ in describing the process of laser heating is clear; z_{D} defined above is the thermal diffusion distance. The temperature dependence of the properties results in a nonlinear equation that is very difficult to solve exactly. Where the functional dependence of these quantities on temperature is known, it is sometimes possible to use numerical integration techniques to obtain a solution. As would be expected, it is extremely difficult to solve the heat flow problem exactly in the general case and so reasonable approximations are used. In addition, only problems that are easy to solve are attempted. These are then useful as guides for solving other problems. Consider the equation of heat conduction in a solid with the laser energy absorbed on the irradiated surface as a heat source. By judiciously selecting the beam geometry, dwell time, and sample configuration, the problem may be reduced to solvable one- and two-dimensional heat flow analyses. Phase transitions can be included and the temperature distributions that are produced can be calculated [7]. Thermal effects play a major role in solid-state lasers, where they cause lensing and polarization coupling through built-in stress and strain fields. The modelling of the thermal problem has been an important issue from the first days of laser science and technology [8]. Numerical modelling remains however a rather long exercise and suffers the usual limitation that there is no insurance that the solution is correct. This is why an analytical treatment of the thermal problem remains interesting. A further interest stems from the fact that a number of laser geometries, such as axially pumped systems, exhibit a circularly cylindrical symmetry, thus lending themselves to an easier analytical analysis. Moreover, a number of structures not showing circular symmetry but pumped axially or radially can be treated on the basis of the assumption of circularly cylindrical symmetry with a reasonably good approximation [2].

2.1 *Source density heat*

Two types of possible pumping method can be tested: Gaussian and top hat beam distribution. They will cause heat generation through the laser medium. For Gaussian beam

distribution, the heat generation through the laser medium ($Q(r, z)$ in W/m^3) can be written as

$$Q(r, z) = \frac{2Q\mu \exp(-2r^2/w_0^2) \exp(-\mu z)}{\pi w_0^2[1 - \exp(-\mu L)]}, \tag{5}$$

where $Q = \eta P$, η is the thermal factor, P is the absorption power (W), w_0 is the waist radius (m), μ is the absorption coefficient (3.50 cm^{-1}), L is the length of the laser rod (m). For uniform power distribution through the beam (top hat), the heat generation through the laser medium can be written as

$$Q(r, z) = \frac{Q\mu \exp(-\mu z)}{\pi a^2[1 - \exp(-\mu L)]}, \qquad r \leq a, \tag{6}$$

where heat generation is zero elsewhere (i.e. the heat generation vanishes when the radius is greater than the pumping beam radius a) [9].

3. Optimization

Swarm intelligence is the study of computational systems inspired by the 'collective intelligence'. Collective intelligence emerges through the cooperation of large numbers of homogeneous agents in the environment. Examples include schools of fish, flocks of birds, and colonies of ants. Such intelligence is decentralized, self-organizing and distributed throughout an environment.

4. Bacterial foraging optimization algorithm (BFOA)

The bacterial foraging optimization algorithm belongs to the field of bacteria optimization algorithms and swarm optimization, and more broadly to the fields of computational intelligence and metaheuristics. The BFOA is inspired by the group foraging behaviour of bacteria such as *E. coli* and *M. xanthus*. Specifically, the BFOA is inspired by the chemotaxis behaviour of bacteria that will perceive chemical gradients in the environment (such as nutrients) and move toward or away from specific signals. Bacteria perceive the direction to food based on the gradients of chemicals in their environment. Similarly, bacteria secrete attracting and repelling chemicals into the environment and can perceive each other in a similar way. Using locomotion mechanisms (such as flagella) bacteria can move around in their environment, sometimes moving chaotically (tumbling and spinning), and other times moving in a directed manner that may be referred to as swimming. Bacterial cells are treated like agents in an environment, using their perception of food and other cells as motivation to move, and stochastic tumbling and swimming-like movement to re-locate. Depending on the cell–cell interactions, cells may swarm a food source, and/or may aggressively repel or ignore each other.

The information-processing strategy of the algorithm is to allow cells to stochastically and collectively swarm toward optimas. This is achieved through a series of three processes on a population of simulated cells: (1) 'Chemotaxis' where the cost of cells is declined by the proximity to other cells and cells move along the manipulated cost surface one at a time (the majority of the work of the algorithm), (2) 'Reproduction' where

only those cells that performed well in their lifetime may contribute to the next generation, and (3) 'Elimination-dispersal' where cells are discarded and new random samples are inserted with a low probability [10].

The bacterial foraging optimization is based on the foraging strategy of *E. coli* bacteria. The foraging theory is based on the assumption that animals obtain maximum energy nutrients E supposing T is a small time. The basic bacterial foraging optimization consists of three principal mechanisms; namely chemotaxis, reproduction and elimination-dispersal. The brief descriptions of these steps involved in bacterial foraging are presented below.

4.1 *Chemotaxis*

During chemotaxis, the bacteria climb the nutrient concentration, avoid noxious substances, and search for a way out of the neutral media. This process is achieved through swimming and tumbling. The bacteria usually take a tumble followed by a tumble, tumble followed by a run, or swim. This movement of bacteria in each chemotaxis step can be expressed by eq. (7)

$$\theta^i(j+1, K, l) = \theta^i(j, K, l) + C(i)\frac{\Delta(i)}{\sqrt{\Delta^T(i)\Delta(i)}}, \tag{7}$$

where $\theta^i(j, K, l)$ represents the position vector of the ith bacterium, in jth chemotaxis step, in kth reproduction step and in lth elimination and dispersal step. $C(i)$ shows the step size taken in the random direction specified by the tumble. $\Delta(i)$ depicts the direction vector of the jth chemotaxis step. When the bacterial movement is run or swim, $\Delta(i)$ is taken as same that was available in the last chemotaxis step; otherwise, $\Delta(i)$ is a random vector whose elements lie in $[-1, 1]$.

4.2 *Reproduction*

Using eq. (8), the health/fitness of the bacteria is calculated.

$$J^i_{\text{health}} = \sum_{j=1}^{Nc+1} J(i, j, k, l), \tag{8}$$

where Nc is the maximum step in a chemotaxis step. During reproduction, all bacteria are sorted in reverse order according to fitness values. The least healthy bacteria die and the rest of the healthy bacteria each splits into two bacteria, which are placed in the same location in the search space. Thus the population of bacteria remains constant. The reproduction process of bacterial foraging aims to speed up the convergence suitable in static problems, but not in dynamic environment.

4.3 *Elimination and dispersal*

The elimination and dispersal events assist chemotaxis progress by placing the bacteria to the nearest required values. In BFO, the dispersion event happens after a certain

number of reproduction processes. Each bacterium, according to a fixed probability, disperses from its original position and moves to the best position within the search space. These events may prevent the local optima trapping but disturb the optimization process. Elimination and dispersal helps to avoid premature convergence or, being trapped in local optima [3].

4.4 *Social communication*

In nature there is the social communication between bacteria such that they are neither close together nor far away from each other. This is done by releasing a chemical by the bacteria. The chemical signal can be either attractant or repellent. If the chemical signal released by a particular bacteria is attractant in nature, then it attracts other bacteria to come to its position. On the contrary if the chemical signal released by a particular bacteria is repellent in nature, it does not allow other bacteria to come to its position. The social communication between bacteria can be simulated using the modified objective function to be computed for the ith position corresponding to the ith position bacteria as given below.

$$J_{\text{mod}}(X^i) = J(X^i) + J_{\text{social}}(X^i), \tag{9}$$

where J_{mod} is the modified objective function computed for the ith position X^i corresponding to the ith bacteria. $J(X^i)$ is the actual objective function value computed for the ith position X^i corresponding to the ith bacteria. $J_{\text{social}}(X^i)$ is the attractant cum repellent signal computed for the ith position X^i corresponding to the ith bacteria as displayed below.

Let

$$d_{ij} = \|X^i - X^j\|^2$$

$$J_{\text{social}}(X^i) = M\left(\sum_{j=1}^{N} \mathrm{e}^{-Rd_{ij}} - \sum_{j=1}^{N} \mathrm{e}^{-Ad_{ij}}\right). \tag{10}$$

Note that if the first term is reduced if the distance between the ith position and others are made large, it acts as the repellent signal. Similarly, the second term $\sum_{j=1}^{N} \mathrm{e}^{-Rd_{ij}}$ is reduced if the distance between the ith position and others are made small, it acts as the attractant signal. R is the repellent factor and A is the attractant factor [11].

4.5 *Heuristics*

(a) The algorithm was designed for application to continuous function optimization problem domains.
(b) Given the loops in the algorithm, it can be configured in numerous ways to elicit different search behaviour. It is common to have a large number of chemotaxis iterations and a small number of other iterations.
(c) The default coefficients for swarming behaviour (cell–cell interactions) are as follows: $d_{\text{attract}} = 0.1$, $w_{\text{attract}} = 0.2$, $h_{\text{repellent}} = d_{\text{attract}}$, and $w_{\text{repellent}} = 10$.

(d) The step size is usually a small fraction of the search space, such as 0.1.
(e) During reproduction, typically half the population with a low health metric are discarded, and two copies of each member from the first (high-health) half of the population are retained.
(f) The probability of elimination and dispersal (P_{ed}) is commonly set quite large, such as 0.25 [10].

5. Output power

As high output power is required, just for instance, for laser machining processes, and the output power of the laser oscillator is not great enough, the radiation will be guided through an amplifier that has to be pumped. Both the radiation to be amplified and the pump radiation heat the amplifier leading to phase change, thermal stresses leading to cracks and variation of the refractive index and under circumstances to vary the plane form of the input and output surfaces of the amplifier. These effects may damage the amplifier or change the front surface of the radiation leading to inaccurate laser machining. To avoid these changes, a pre-study of the spatial and temporal temperature distribution has to be carried out in linear and nonlinear media. The results of this study will be later applied in equations concerning the thermal stresses, the results of which will be necessary to determine the variation of the refractive index. With the aid of Maxwell equations, the wave propagation in such an optically deformed amplifier will be determined. From the obtained results we hoped to find a way to correct the front surface of the wave thereby increasing the accuracy of laser machining [6]. The volumetric heating of the laser material by the absorbed pump radiation and surface cooling required for heat reduction leads to a non-uniform temperature distribution in the material. This results in a distortion of the laser beam due to the temperature- and stress-dependent variation of the index of refraction. Thermal stress-induced birefringence and thermal lensing effects in rod-shaped materials have been a big issue for realizing high performance solid-state lasers [12]. The starting point for analysing the thermal aspects of laser–tissue interactions is to define and understand the system of interest. In the most general sense, a system is identified as that portion of the Universe that is involved directly in a particular process. The remainder of the Universe is called the environment. The system interacts with the environment across its boundary. These interactions are directly responsible for changes in the state of the system. The boundary surface provides a locus at which interactions can be identified and accounted for so as to predict the resulting changes in the system. The temporal boundary condition is generally defined in terms of a known temperature distribution within the system at a specific time, usually at the beginning of a process of interest. However, definition of the spatial boundary conditions is not so straightforward. There are three primary classes of spatial boundary conditions that are encountered most frequently. The thermal interaction with the environment at the physical boundary of the system may be described in terms of a defined temperature, heat flux, or convective process. The simplest specification for each of these conditions is that it remains constant over time, which leads to the most simple mathematical expression for the boundary condition. However, if the actual process of interest precludes using a constant boundary

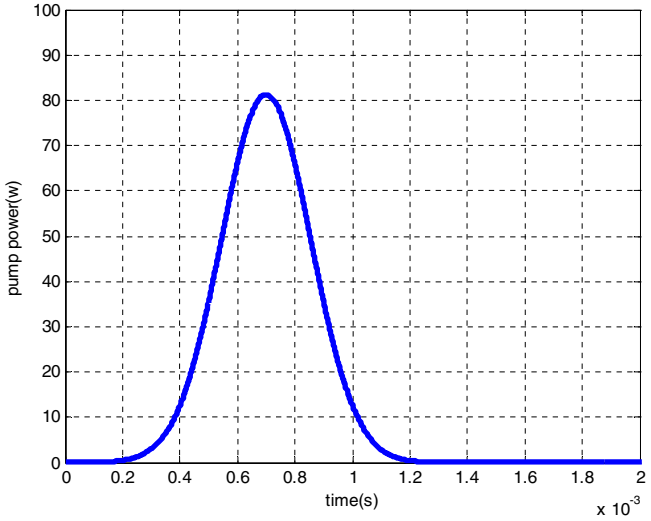

Figure 1. The output pump power from the laser diode.

condition, as may be encountered in biological applications, then a more complex specification is required that may require a numerical solution [13]. The laser output power P_{out} is related to the photon number φ by the simple relation:

$$P_{\text{out}} = \frac{\gamma^2}{2\gamma}(h\nu)\frac{\varphi}{\tau_{\text{c}}} = \frac{\gamma^2 c}{2L_{\text{e}}}h\nu\varphi. \tag{11}$$

In fact, $(h\nu)(\varphi/\tau_{\text{c}})$ is the total EM energy lost in the cavity per unit time, and solely a fraction $\gamma^2/2\gamma$ of this power is available due to the transmission through the output

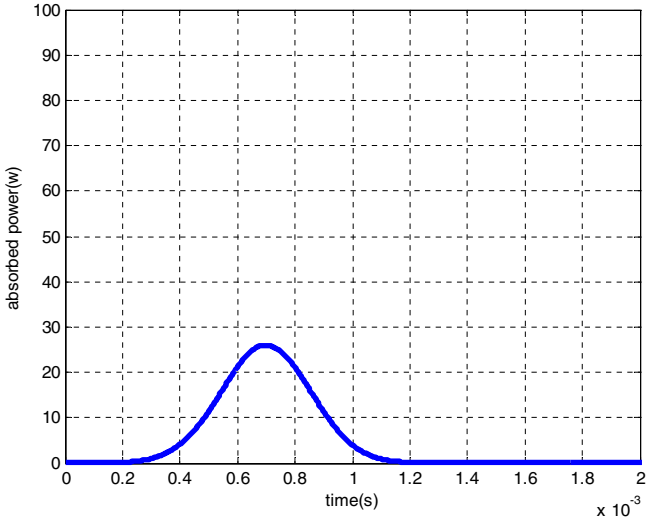

Figure 2. The absorption pump power.

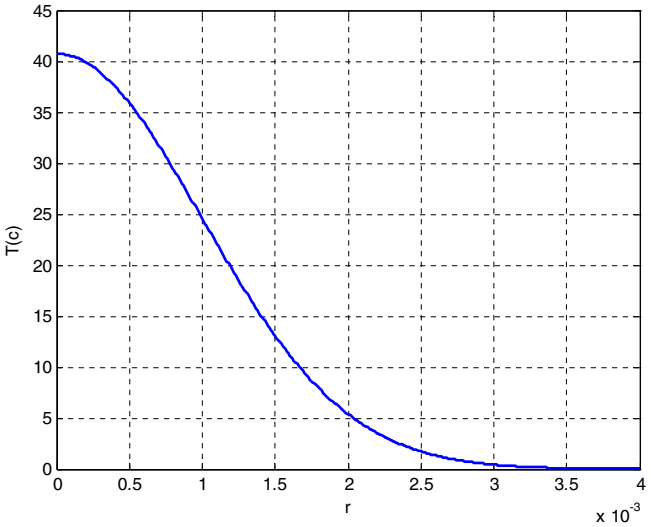

Figure 3. The relation between r and T for the Gaussian heat source.

mirror. For a typical CW laser operated in the continuous-wave regime, the number of photons φ stored in the cavity may vary from about 10^{10} photons for low-power lasers (such as a HeNe laser delivering $P_{\text{out}} = 10$ mW power at $\lambda = 632.8$ nm) to 10^{17} photons for high-power lasers (such as a CO_2 laser delivering an output power $P_{\text{out}} = 10$ kW at $\lambda = 10.6$ μm). The corresponding output laser power can then be calculated from the following equation:

$$P_{\text{out}} = \eta_{\text{s}}(P_{\text{p}} - P_{\text{th}}), \tag{12}$$

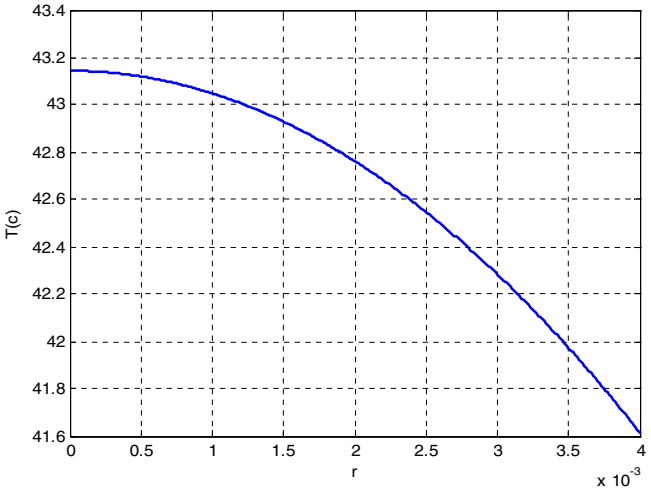

Figure 4. The relation between r and T for the top hat heat source.

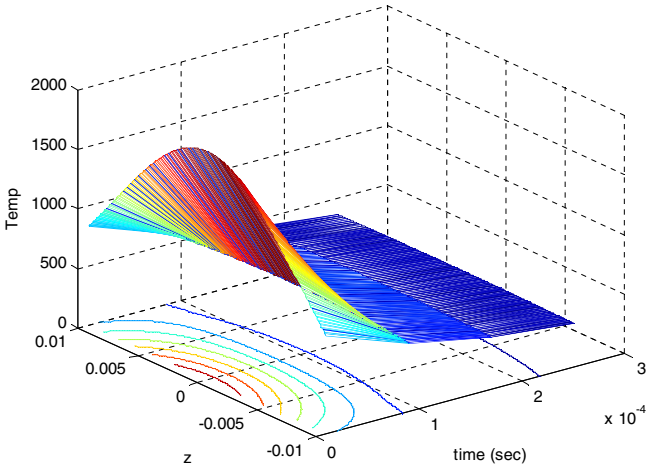

Figure 5. The time dependence of the temperature induced by the pump beam calculated at any z value.

where

$$\eta_s = \eta_p \eta_c \eta_q \eta_t. \tag{13}$$

Equation (13) shows that, within the approximation made, a linear relation is obtained between the output power and the pump power. One can then define the slope efficiency of the laser as $\eta_s = dP_{out}/dP_p$. According to (12), η_s is given by the product of four contributions, the pump efficiency η_p, the output coupling efficiency $\eta_c = \gamma^2/2\gamma$, the laser quantum efficiency $\eta_q = h\upsilon/h\upsilon_{mp}$ and the transverse efficiency $\eta_t = Ab/A$, where

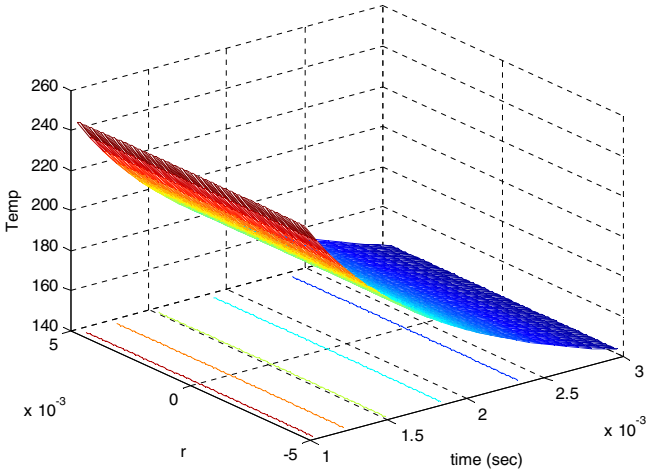

Figure 6. The time dependence of the temperature induced by the pump beam calculated at any r value.

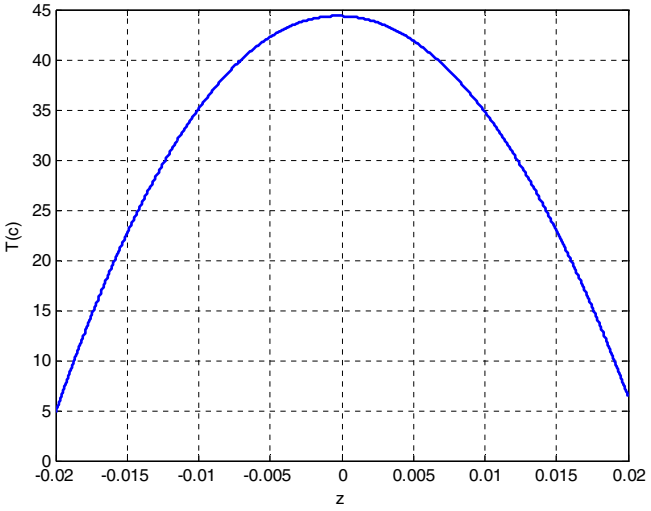

Figure 7. Thermal distribution through the length of the rod ($z = 20$ mm) at Gaussian heat source.

$Ab = Va/l$ is the transverse mode area in the active medium and A is the transverse pumping area. The slope efficiency of a laser may typically vary from less than 1% in low-efficiency lasers (such as in the HeNe laser) to 20–50% or even higher in high-efficiency lasers [14].

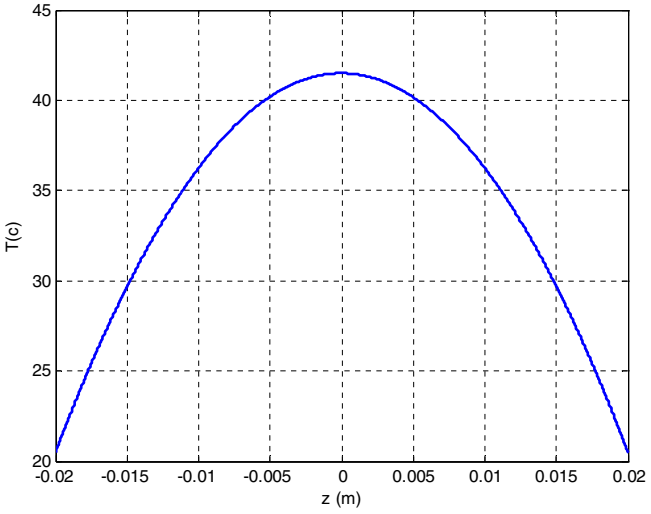

Figure 8. Thermal distribution through the length of the rod ($z = 20$ mm) at top hat heat source.

5.1 *Threshold pump power*

Once the threshold value of the pump rate is calculated, we can readily obtain the corresponding threshold pump power. We get in fact the following expression:

$$P_{\text{th}} = \left(\frac{\gamma}{\eta_{\text{p}}}\right)\left(\frac{h\nu_{\text{p}}}{\tau}\right)\left[\frac{\pi\left(w_0^2 + w_{\text{p}}^2\right)}{2\sigma_{\text{e}}}\right] \tag{14}$$

which hold for longitudinal pumping. Note that, again for longitudinal pumping, the threshold pump power increases as w_0 increases because, as w_0 increases, the wings of the mode extend further into the less strongly pumped regions of the active medium [15].

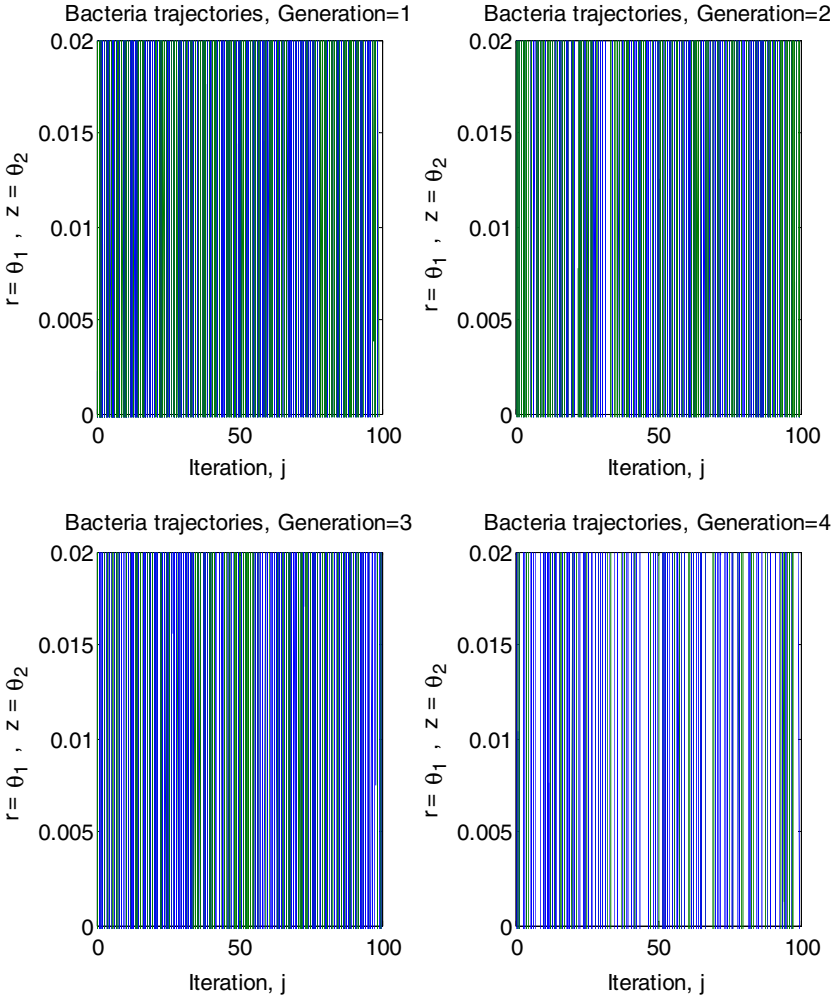

Figure 9. The motion trajectories of the bacteria on the contour plot of function in figure 5.

6. Computer simulations

The simulation has been used to obtain temperature distribution and displacement across continuous pumped Nd:YAG laser rod of 1064 nm. The rod was end pumped from two ends and it has been tested with pump power ranging from 20 to 80 W for radius pumping ratios of $1/2$, $1/3$, and $1/4$, for both top hat and Gaussian beam pumping. A Gaussian beam diameter of 300 μm has been chosen. The pumping power at 80 W and a radius pumping ratio of $1/2$ is shown in figure 1. It shows Gaussian beam pumping with time where the pulse width of the pumping $=$ 1 ms. The absorption power from the crystal is

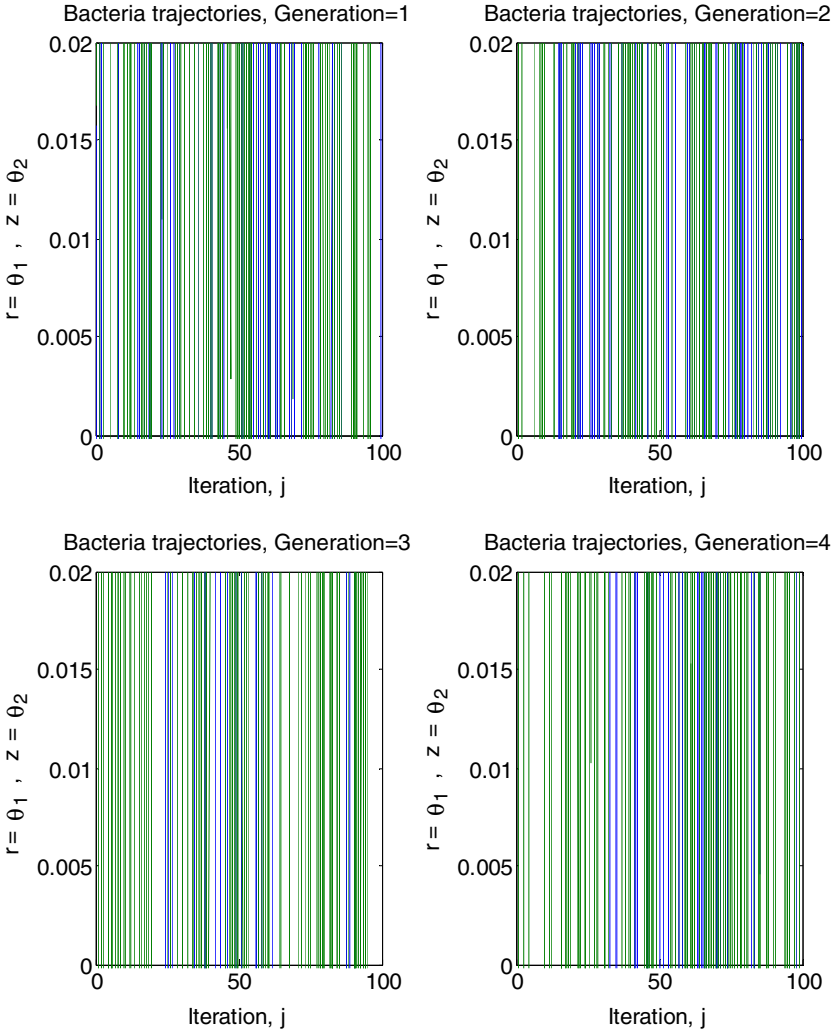

Figure 10a. The motion trajectories of the bacteria on the contour plot of function in figure 6.

calculated from the relation $P_{\text{abs}} = 0.32 P_{\text{pump}}$, and the absorption power is described in figure 2.

Before presenting the results of bacterial swarm intelligence simulation, we discuss a simpler steady-state temperature distribution in symmetrical cylindrical rod with radially symmetric heating distributions. In this case, eq. (2) can be written as

$$\frac{1}{r}\left[k\frac{\partial}{\partial r}\left(r\frac{\partial T}{\partial r}\right)\right] + k\frac{\partial^2 T}{\partial z^2} + Q(r,z) = 0, \tag{15}$$

where T is the temperature distribution in °C, $Q(r,z)$ is the heat source density that is a function of the pump power density, r and z are the radial and longitudinal coordinates and k is the thermal conductivity of Nd:YAG laser rod. The Nd:YAG rod has a radius of 4.75 mm and a length L of 20 mm. The heat transfer coefficients for the

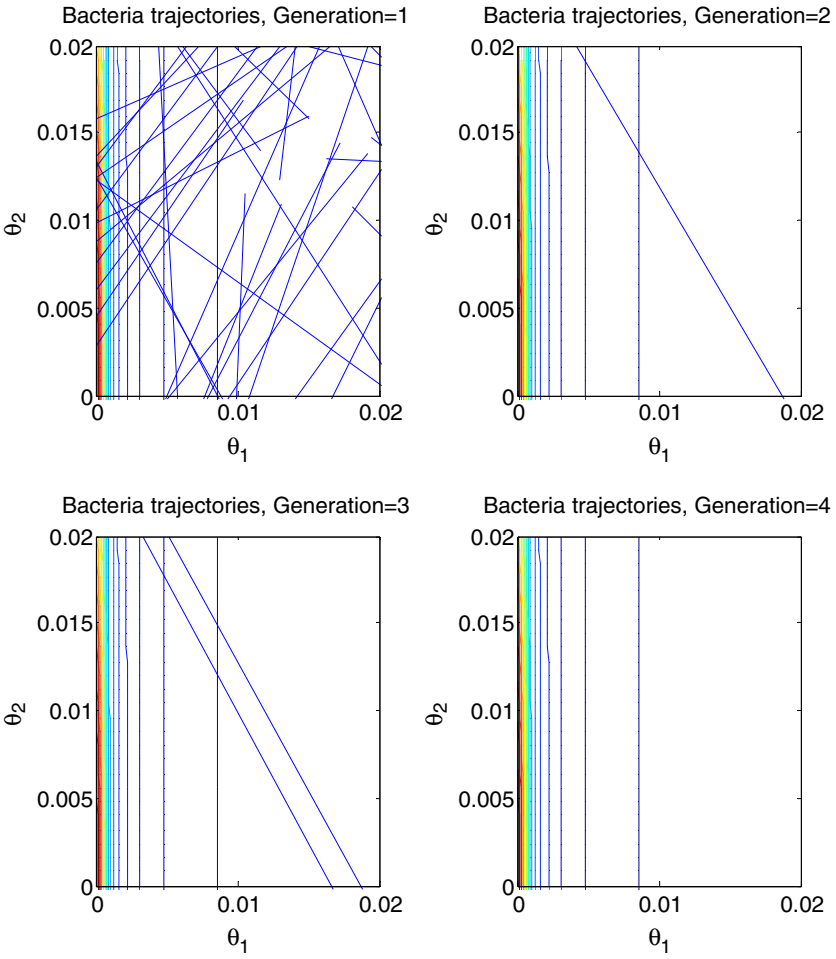

Figure 10b. The algorithm explores other regions of the optimization domain for function in figure 5.

surfaces in contact with water and air, respectively are $h_w = 0.67$ W·cm^{-2}·K^{-1} and $h_a = 0.005$ W·cm^{-2}·K^{-1}. The total pump power of 80 W has an absorption coefficient of 3.5 cm^{-1}. The thermal conductivity of Nd:YAG is 13 W·m^{-1}·K^{-1}. For Gaussian heat source the relation between thermal distribution and radius of laser rod is shown in figure 3. For top hat heat source the relation between the thermal distribution and the radius of laser rod is shown in figure 4. Figure 5 represents the time dependence of the temperature induced by the pump beam calculated at any z value. The temperature increases as the irradiation time of the pump beam increases. It reaches its maximum value at $t = 1 \times 10^{-3}$ s which is greater than the time at which the intensity of the pump beam is maximum. Figure 6 represents the time dependence of the temperature induced by the

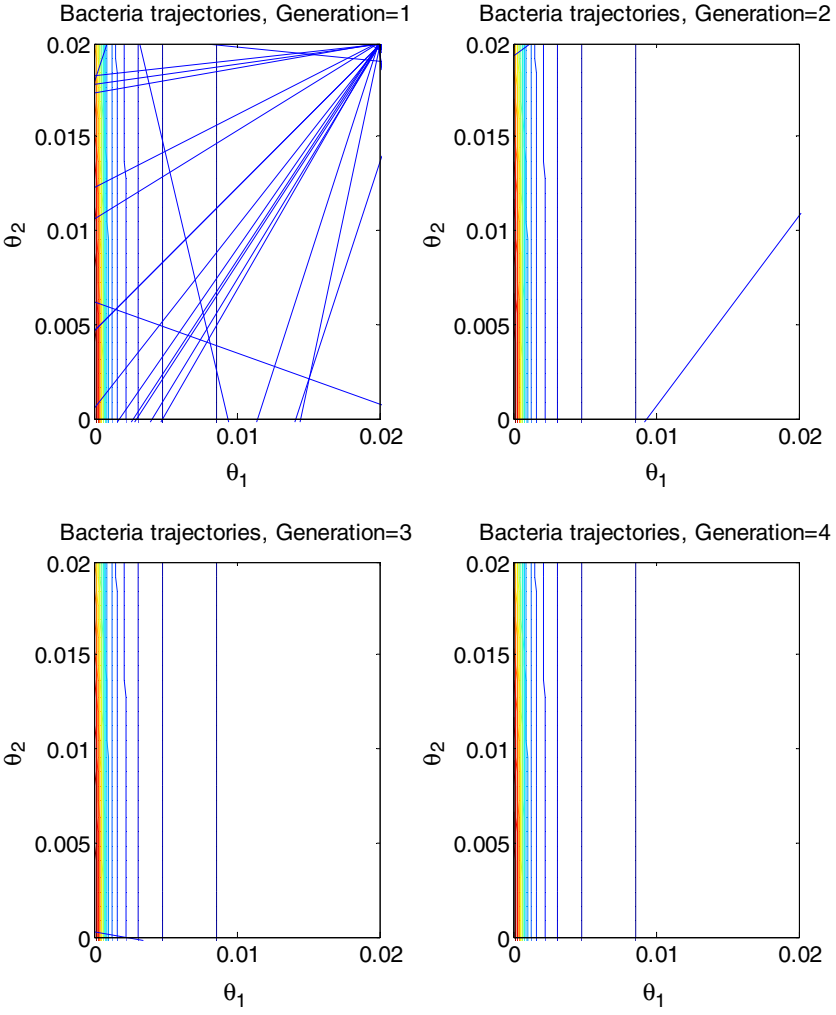

Figure 11. The algorithm explores other regions of the optimization domain for function in figure 6.

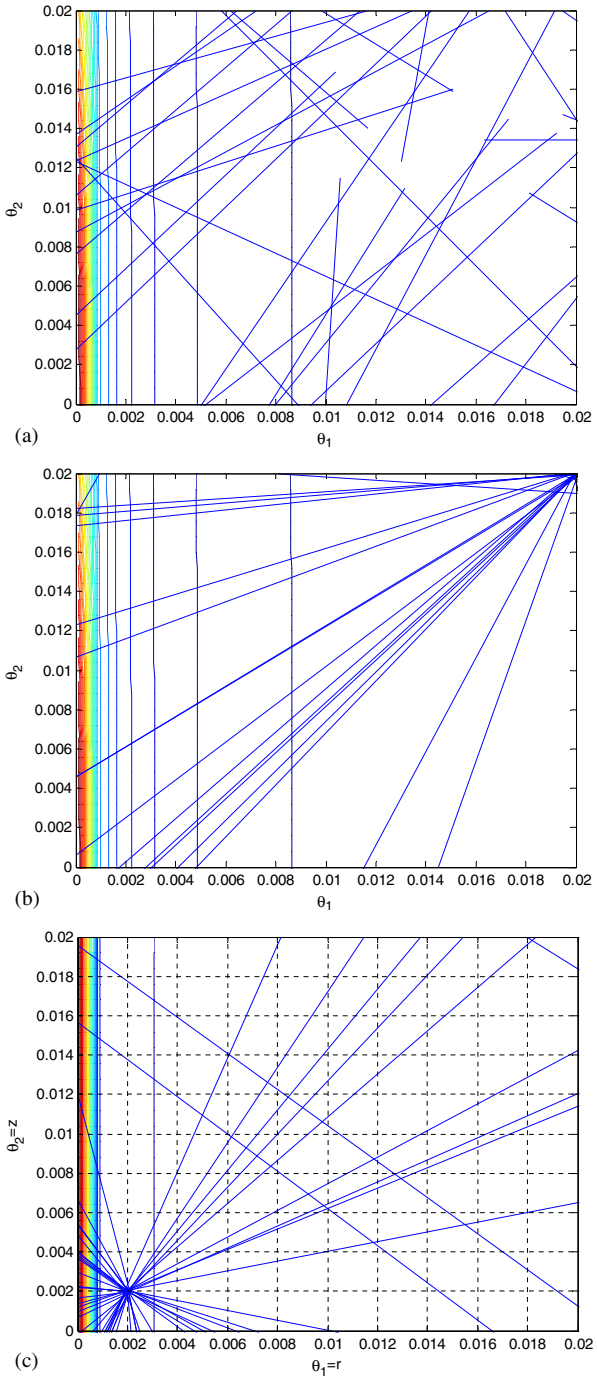

Figure 12. Bacterial movements through the search space toward the global minima. (**a**) Initial movement, (**b**) movement after 15 iterations and (**c**) final movement.

pump beam calculated at any r value. The thermal distribution through the length of the laser rod for Gaussian and top hat heat sources at steady state are shown in figures 7 and 8 respectively.

BFOA that allows simulating different cases of the laser rod heated by the continuous pumping with different space distributions of the pump power, was developed. We use the algorithm to find the minimum of the function in figures 5 and 6 respectively. We assume that this surface can be sampled, but that the gradient is not known. The bacteria are initially spread randomly over the optimization domain. The results of the simulation are illustrated by motion trajectories of the bacteria on the contour plot of function in figures 5 and 6 as shown in figures 9, 10a and 10b in the first generation, starting from their random initial positions, searching is occurring in many parts of the optimization domain, and we can see the chemotactic motions of the bacteria as the black trajectories where the peaks are avoided and the valleys are pursued. Reproduction picks the 25 healthiest bacteria and copies them, and then, as shown in figures 9, 10a and 10b in generation 2, all the chemotactic steps are in five local minima. This again happens in going to generations 3 and 4, but bacteria die in some of the local minima, so that in generation 3, there are four groups of bacteria in four local minima, whereas in generation 4, there are two groups in two local minima. Next, with the above choice of parameters, there is an elimination-dispersal event, and we get the next four generations shown in figures 10a, 10b and 11. Notice that elimination and dispersal shift the locations of several of the bacteria thereby the algorithm explores other regions of the optimization domain. However, qualitatively we find a similar pattern to the previous four generations where chemotaxis and reproduction work together to find the global minimum; this time, however, due to the large number of bacteria that were placed near the global minimum, after one reproduction step, all the bacteria are close to it (and remain this way). In this way, the bacterial population has found the global minimum. The final bacterial movement to explore the

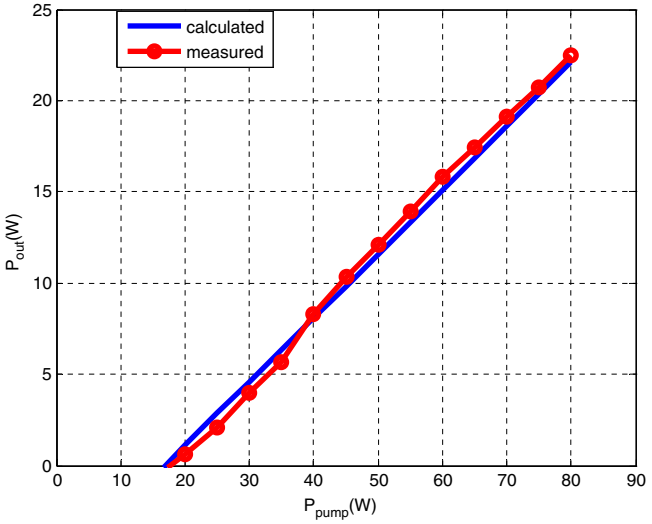

Figure 13. The output pump power from the laser rod.

global minima is described in figures 12a, b and c. The output power with change in incident pump power is given in figure 13. The output laser had a threshold of 18 W. The maximum power output from the Nd:YAG laser was 22.5 W for 80 W of incident pump power. This gives an approximate slope efficiency of 52%.

7. Results and discussion

Figures 3 and 4 show that Gaussian beam pumping will increase the temperature distribution more than the top hat beam, especially, at the central portion of the rod. As the time of irradiation increases the temperature increases and a greater gradient at $r = 0$ will build up. But because of the bad heat conductivity and the relatively small pulse duration, the conducted energy remains small. This process lasts until the time at which the rate of the conducted heat energy into the cooler zones is equal to the rate of the energy of the absorbed radiation. At this time, the temperature reaches its maximum and after that the rate of the losses overcompensate the absorbed radiation and the temperature begins to decrease. Because of the great temperature gradient at the beginning of its reduction, the temperature decreases with a great slope followed by a smaller one till the end of the pump beam. Reduced thermal stress and strain held thermal tensing and enhance beam quality. The software developed by us makes it possible to set arbitrary heat conductivity coefficients along different axes in the crystal block. In this case, the distribution of temperature is different along the r- and z-axes. Therefore, the thermally-induced lens is astigmatic in this case. The astigmatism of the thermal lens can be reduced using elliptical pump beam.

8. Validation

The simulation found above will be compared with the results obtained by analytical solution. The validity of the analytical solution for thermal problems has been evaluated and confirmed in ref. [4] and can, therefore, be used as a reliable reference. Reference [4] reports on the validation of an analytical solution under the conditions which are considered in the present paper (cooling configuration, geometry, boundary conditions, shape of the pump beam along the transverse axis, etc.). From simulations it can be seen that the maximum temperature is at the centre of the crystal rod. The temperature distributions for the Gaussian and top hat beams strongly differ only in the inner region of pump beams. The temperature distributions practically coincide in the outer region of the beams inside the rod, though analytical expressions for temperature distribution are very different. We found that the temperature gradient for the Gaussian beam is smaller than for the top hat pump beam. In order to verify the validity of the algorithm we proposed, experiment for the parameter of bacterial foraging optimization algorithm is as follows. We choose $S = 30$, $N_{\mathrm{ed}} = 2$, $N_{\mathrm{re}} = 4$ and $N_{\mathrm{c}} = 50$. By an implementation based on the description of the seminal work, we validate our model and the computational interpretation of swarms with algorithms implementing collision-based aggregation, collective perception, emergent taxis, foraging, and 'random-tree' aggregation. The use of our program allows

us to optimize experimental arrangement of the laser oscillator or the amplifier and to improve performance of the constructed laser system.

9. Conclusions

A new simulation algorithm modelling of the thermal problem in laser rods with circularly cylindrical symmetry was derived, taking into account an inhomogeneous heat source of the pumping beam along the propagation axis inside the laser rod. Comparison with analytical solution and FE simulations shows an excellent agreement. The BFOA method can be generalized to any cooling configuration as long as it has a circular symmetry. The heating function was assumed to have a Gaussian and top hat transverse distribution but the proposed simulation method can be extended to many transversal shapes. In all practical cases, the solution of partial differential equations can be obtained in the form of integrals, but in many cases these integrals are not easy to implement. The BFOA based on analytical expressions obtained for the temperature distribution open the way to a better physical understanding of thermal phenomena and represent a fast tool for solid-state laser design and optimization. The same method can be implemented for obtaining the stress distribution and the thermally-induced birefringence in heated laser rods.

References

[1] J K Jabczyñski, J Jaguoe, W Endzian and J Kwiatkowski, *Opto-Electron. Rev*. **13(1)**, 69 (2005)
[2] Boris A Usievich and Vladimir A Sychugov, Florent Pigeon and Alexander Tishchenko, *IEEE J. Quantum Electron*. **37**, 1210 (2001)
[3] Veysel Gazi and Kevin M Passino, *Swarm stability and optimization* (Springer Science + Business Media B.V., 2011)
[4] B K Panigrahi, Y Shi and M-H Lim (eds.), *Handbook of swarm intelligence: Concept principles and application* (Springer-Verlag, Berlin, Heidelberg, 2011)
[5] W A Clarkson, *Appl. Phys*. **34**, 2381 (2001)
[6] M M El-Nicklawy, A F Hassan, El M A Nasr, A A Hemida, S L Diab and S M El-Genedy, *Egypt. J. Solids* **31**, 231 (2008)
[7] Michael Bass and Aravinda Kar, *Encyclopedia of physical science and technology* (Springer, Berlin, 2011)
[8] V A Sychugov, V A Mikhailov, V A Kondratyuk, N M Lyndin, Y Fram, A I Zagumennyi, Y D Zavartsev and P A Studenikin, *Quantum Electron*. **30**, 13 (2000)
[9] Khalid S Shaibib, Mohammed A Minshid and Nebras E Alattar, *Thermal Science* **15**, 399 (2011)
[10] Jason Brownlee, *Clever algorithms: Nature inspired recipes* (2011)
[11] E S Gopi, *Mathematical summary for digital signal processing application with matlab* (Springer Science+Business Media B.V., 2010)
[12] Koji Sugioka, Michel Meunier, Alberto Piqué, *Laser precision microfabrication* (Springer-Verlag, Berlin, Heidelberg, 2010)
[13] Ashley J Welch, Martin J C van Gemert, *Optical thermal response of laser-irradiated tissue*, 2nd edn (Springer Science+Business Media B.V., 2011)
[14] Frank Träger, *Springer handbook of laser and optics* (Springer Science+Business Media, LLC New York, 2007)
[15] Orazio Svelto, *Principles of laser* (Springer Science+Business Media, LLC, 2010)